AI-based thermal bridge detection of building rooftops on district scale using aerial images

Zoe Mayer M.Sc.[a]*, Yu Hou M.Sc[b], Dr. James Kahn[c], Dr. Rebekka Volk[a],
Prof. Dr. Frank Schultmann[a]
[a] Karlsruhe Institute of Technology, Germany, [b] University of Southern California, USA, [c] Helmholtz AI, Karlsruhe Institute of Technology, Germany
zoe.mayer@partner.kit.edu

Abstract. Thermal bridges are weak areas of building envelopes that conduct more heat to the outside than surrounding envelope areas. They lead to increased energy consumption and the formation of mold. With a neural network approach, we demonstrate a method of automatically detecting thermal bridges on building rooftops from panorama drone images of whole city districts. To train the neural network, we created a dataset including 917 images and 6895 annotations. The images in the dataset contain thermal information for detecting thermal bridges and a height map for rooftop recognition in addition to regular RGB information. Due to the small dataset, our approach currently only has an average recall of 9.4% @IoU:0.5-0.95 (14.4% for large objects). Nevertheless, our approach reliably detects structures only on rooftops and not on other parts of buildings, without any additional segmentation effort of building parts.

1. Introduction

In 2017, building constructions and operations accounted for 36% of global final energy use worldwide and about 40% of energy-related carbon dioxide emissions (GlobalABC, 2018). Thermal energy is a particularly relevant component of this: more than a half of current global household energy use is for space and water heating (IEA, 2014). In addition to high energy standards for new buildings, the energy retrofit of old buildings plays an important role. While new construction adds annually 1% or less to the existing building stock, the other 99% of buildings already existed in the year prior (Power, 2008).

To develop energy-saving approaches for existing buildings in cities, strategies on different aggregation levels can be considered: at the single building scale, the district scale, and the full-city scale. The district scale, the intermediate level between the city and the building scale, is coming increasingly into the focus of building science and urban transition planning. The main strengths of the district scale for the building energy retrofit are summarized by Riechel (2016): Compared to measures for single buildings, measures for whole districts provide the possibility of cost digressions and other economies of scale for energy improvements. For example, the planning and implementation of retrofit measures such as the purchase of retrofit material can be cheaper for a large demand in a small area at the same time. Compared to the city scale, the closeness between habitants and building owners contributes to neighborhood-dynamics in districts. Informal communication among neighbors ("neighborhood gossip") or the copying of a building retrofit in the neighborhood by other owners can have benefits for implementing energy improvement measures. (Riechel, 2016)

There are approaches to systematically use the advantages of the district scale to push urban transition and the retrofit of buildings. One of the most frequently practical and standardized approaches in this field is from Germany called “energetisches Quartierskonzept” (EQ). It describes a policy plan that intends to improve the energy quality of private and public buildings and the energy infrastructure of a whole city district. So far, more than 1,000 EQs have been financially supported by the German government (BES, 2020).

To identify districts with a high need for energy retrofits and to develop effective measures for substantially improving the energy quality of a district, an initial thermal quality analysis of existing buildings is necessary. Currently, such analyses on district scale are expensive and time consuming (Riechel et al., 2016; Neußer, 2017). Therefore, approaches that allow for automatic and simplified analyses are crucial for a higher efficiency of EQs and other retrofit planning approaches.

With the help of unmanned aerial vehicles (UAV, drones), it is possible to collect thermal panorama images of many buildings from different angles with relatively little effort and cost but with a high resolution. A distinction is made between quantitative and qualitative thermography. In quantitative thermography, absolute temperatures are measured as precisely as possible. The process is highly dependent on environmental parameters, the infrared camera used, and the qualifications of the thermography staff. Qualitative thermography, on the other hand, is simpler. It focuses on temperature distributions and differences. Thermal bridges in particular can be easily identified in qualitative images. (Volland et al., 2016)

A thermal bridge is an area of the building envelope that conducts heat easily, thus transporting heat from the warmer inside to the colder outside faster than it does through the adjacent areas. This is caused by different thermal conductivities of used materials or the geometry of constructions. Air leaks can also be subsumed under the term thermal bridge (Schmidt and Windhausen, 2018). Thermal bridges cause high energy losses which can make up to one third of the transmission heat loss of an entire building. Additionally, they lead to the collection of moisture, which in the long term degrades the building fabric or causes mould. A thermal bridge can be seen on a thermographic image as an area with an increased thermal radiation relative to adjacent areas. (Schild, 2018).

2. Research approach

In this study, we analyse how drone-based thermal images can be used for a simple analysis of the thermal quality of building envelopes on district scale. To do so, we investigate the quality of thermal panorama images obtained by drones and analyse how artificial intelligence can help to automatically detect thermal bridges. We focus on thermal bridges on rooftops as they are difficult to access with conventional thermography from terrestrial images.

To motivate our research, we first provide an overview about which publications and studies are known to us in the field of automated computer vision approaches to detect thermal bridges of buildings. We focus on studies that work with imagery data obtained by non-stationary recording approaches - especially with drones - suitable for recording images on district scale.

In the main part of our work, we demonstrate a method to automatically detect thermal bridges on building rooftops in thermal aerial images using a neural network. We employ existing solutions from the domain of object detection to learn to identify the size and location of thermal bridges within each image. For this, we create a dataset of drone images with annotations of thermal bridges on building rooftops. Each image of the dataset consists of a combination of a thermal image, an RGB[1] image recorded from the same angle and converted to the same format, and height information for each pixel (Hou et al., 2021 - a). We select a training dataset for the neural network composed of a subset of the images, and validate our results on the remainder of the dataset.

[1] Red, Green, Blue

3. Related work

Non-stationary thermography with the help of cars and drones for the analysis of buildings is becoming increasingly important in thermography studies. The advantage of drones compared to terrestrial methods is that the entire envelope of buildings (including rooftops) can be thermographically assessed. In addition, the influence of facade covering (e.g. by trees or pedestrians walking past) is less prevalent from the bird's eye view.

Publications in the field of automated thermal bridge detection from thermal images obtained with non-stationary cameras are from Garrido et al. (2018), Macher et al. (2020), Martinez-de Dios and Ollero (2006), and Rakha et al. (2018). To automatically detect thermal bridges these publications work with different threshold approaches for temperature differences in the images. They record close-up images of single buildings from different angles, but do not work with panorama images that cover multiple buidlings. Moreover, they use small datasets to validate their approaches and do not focus on entire districts. Garrido et al. (2018) place an infrared camera on the roof of a vehicle to record images at an angle of 45°. The proportion of unrecognized or incorrectly declared thermal bridges is 32% for a test set of three images. Macher et al. (2020) also install their infrared camera on a vehicle and conclude being able to reliably detect thermal bridges between floors and under balconies. No quantitative information is given on the precision of the used algorithm. Martinez-de Dios and Ollero (2006) use a thermal camera placed on a drone helicopter. According to the authors this approach is suitable for detecting thermal bridges on windows. The study lacks precise quality information for evaluating the results. Rakha et al. (2018) also use a drone with a thermal camera to record close-up images of buildings from the air. They state the overall precision of their algorithm of about 75%.

As thermal panorama images contain many different buildings from changing angles and infrastructure in between (e.g. trees, trams, cars, streets, street lights) classic threshold approaches appear unsuitable for the automatic detection of thermal bridges. This is because thermal bridges change in shape from different angles and high temperature differences often occur on objects in the image which are not buildings. For successful thermal bridge detection on panorama images deep learning approaches are very promising, as complex objects such as buildings, certain building parts on that thermal bridges occur (e.g. rooftops), and various thermal bridge types with different shapes can be recognized.

A recent study by Kim et al. (2021) works with a deep learning approach to detect thermal bridges from terrestrial thermographic images. The study uses a method including thermal anomaly area clustering, feature extraction, and an artificial-neural-network-based thermal bridge detection. The average precision of the detection of thermal bridges is for eight test images 89%. However, the images used are close-ups of buildings and cannot be compared to panorama images. To the best of our knowledge there is no study that aims to detect thermal bridges in an entire district on thermal panorama images using deep learning approaches.

4. Dataset

Our dataset of Thermal Bridges on Building Rooftops (TBBR dataset) consists of combined RGB and thermal panorama drone images with a height map (Figure 1). The raw images for our dataset were recorded with a normal (RGB) and a FLIR-XT2 (thermal) camera on a DJI M600 drone. We converted all images to a uniform format of 2400x3200 pixels. They contain RGB, thermal, and GPS information as well as flight altitudes (between 60-80m above ground). The GPS and flight altitude information were used to reconstruct a 3D model out of

the 2D images to create the height map. We hypothesize that this will significantly simplify the task of learning to ignore street-level sections of the images and focus instead on rooftops.

The drone images show parts of the Karlsruhe city centre, east of the market square. The recorded area can be divided into six large city blocks of around 20 buildings per block. Because of a high overlap rate of the images, the same buildings are on average about 20 times on different images, recorded from different angles. The dataset contains a total of 5698 images before preselection. During preselection, all images containing no thermal bridges were filtered out, as well as images that are blurred due to rapid turns or other fast movements of the drone. A total of 917 images remain after preselection.

All images were recorded during a drone flight on March 19, 2019 from 7 a.m. to 8 a.m. At this time, temperatures were between 3.78 ° C and 4.97 ° C, humidity between 80% and 98%. There was no rain on the day of the flight, but there was 2.3mm/m² 48 hours beforehand.[2] For recording the thermographic images an emissivity of 1.0 was set. The global radiation during this period was between 38.59 W / m² and 120.86 W / m², hence the solar radiation was high enough to visually classify the geometric and structural conditions on the RGB images, but not so high that the surface temperatures of thermal bridges and surrounding components change significantly, thus making it difficult to identify thermal bridges. No direct sunlight can be seen visually in any of the recordings.

Figure 1: Drone images of the city centre of Karlsruhe used for the TBBR dataset A) thermal image B) RGB image C) image with height information (height map)

The annotated images of the TBBR dataset contain a total of 6895 annotations. The annotations only include thermal bridges that are easily identifiable, and thus also include thermal bridges that are not annotated. Because of the image overlap each thermal bridge is annotated on average about 20 times from different angles. An example image with annotations is shown in Figure 2. We have published the dataset with further information in Mayer et al. (2021).

[2] The total absence of moisture can therefore not be fully guaranteed. Moisture falsifies the recording of thermographic images. We recognized puddles on some flat rooftops and removed corresponding images from the dataset during the preselection process; otherwise we could not detect any significant moisture visually on the RGB images.

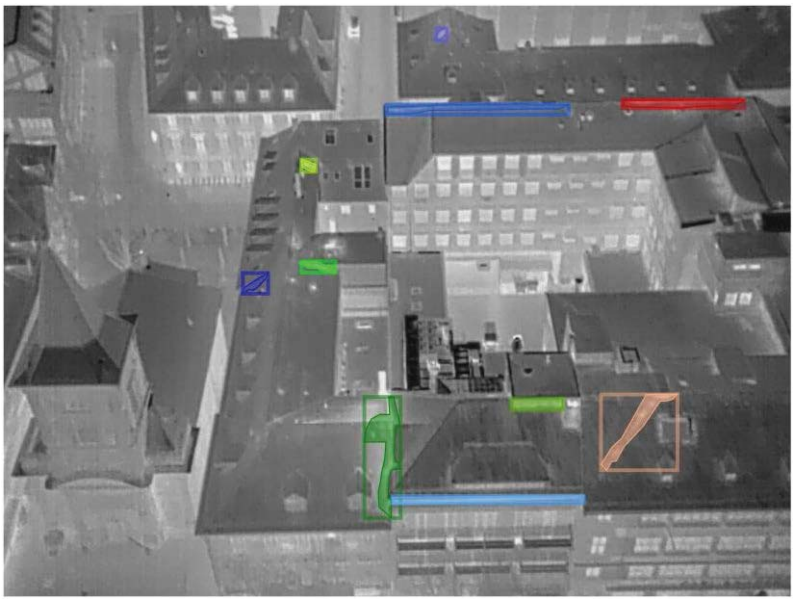

Figure 2: Example of thermal bridge annotations in the TBBR dataset for the example shown in Figure 1. Colours are only for clarity and do not have any other meaning.[3]

5. Experimental procedure

5.1 Data pre-processing

To prepare the datasets, we align thermal images and height images onto RGB images via a process called image registration (Hou et al., 2021 - a). Since on the collected images, fisheye effects occur (called radial distortion) and the lens is not aligned parallel to the imaging plane (called tangential distortion), we must resolve these two distortions before image registration. Distortions can be solved by $x_{corr,rad} = x(1 + k_1r^2 + k_2r^4 + k_3r^6)$ -$y_{corr,tang} = y + [p_1(r^2 + 2y^2) + 2p_2xy]$). In these equations, (x, y) represents a point before correction, and (x_{corr}, y_{corr}) represents a point coordinate after correction. Many collected pairs of coordinates of (x, y) and (x_{corr}, y_{corr}) from a collection of calibration images enable the calculation of the distortion coefficients $(k_1, k_2, k_3, p_1, p_2)$. The coefficients (k_1, k_2, k_3) are radial distortion coefficients and (p_1, p_2) are tangential distortion coefficients.

$$x_{corr,rad} = x(1 + k_1r^2 + k_2r^4 + k_3r^6) \quad (1)$$

$$y_{corr,rad} = y(1 + k_1r^2 + k_2r^4 + k_3r^6) \quad (2)$$

$$x_{corr,tang} = x + [2p_1xy + p_2(r^2 + 2x^2)] \quad (3)$$

$$y_{corr,tang} = y + [p_1(r^2 + 2y^2) + 2p_2xy] \quad (4)$$

After undistorting all images, we aligned thermal and height images onto the RGB images using $[x_{thermal}, y_{thermal}] = T_{RGB \to thermal} * [x_{RGB}, y_{RGB}]$ - $[x_{thermal}, y_{thermal}] =$

[3] The borders of the thermal bridge annotations show a slight distortion. The reason for this lies in the data pre-processing and is explained and discussed in more detail in Section 7.

$T_{height \to thermal} * [x_{height}, y_{height}]$. In these equations, $T_{RGB \to thermal}$ and $T_{height \to thermal}$ represent transformation matrices that transform pixels from RGB images to thermal images and pixels from height images to thermal images.

$$[x_{thermal}, y_{thermal}] = T_{RGB \to thermal} * [x_{RGB}, y_{RGB}] \quad (5)$$

$$[x_{thermal}, y_{thermal}] = T_{height \to thermal} * [x_{height}, y_{height}] \quad (6)$$

Lastly, we connected the registered thermal and height images to the RGB images to produce single 5-channel images (RGB + thermal + height).

5.2 Neural network details

To identify thermal bridges, we employed a neural network to perform object detection and segmentation. Formally, the task is defined as follows: given a set X containing input images $x_i \in R^{N*H*W*C}$, with image height H, width W, and channels C; and a corresponding annotation set Y containing bounding boxes $y_{i,box} \in R^{N*4}$, where 4 represents the coordinates of the box's four corners, class labels $y_{i,cls} \in R^N$, and masks $y_{i,mask} \in R^{N*H*W}$, where N is the number of annotated object in the given image; learn the mapping $F: X \to Y$, where F denotes a neural network.

In this work the neural network is the Mask R-CNN framework (He et al., 2017) with a ResNet-18 (He et al., 2016) backbone implemented in the Detectron2 software package (Wu et al., 2019). We select this architecture for two key reasons: firstly, the ResNet architecture has consistently proven to perform at state-of-the-art (SOTA) levels (e.g. as in Bello et al. (2021)); and secondly, self-supervised training methods offer a means of achieving SOTA performance with limited labelled samples. The latter point is discussed further in section 7 and motivates the use of a neural network over classical approaches.

Figure 3 shows the basic structure of Mask R-CNN. It consists of two stages: the first uses a Region Proposal Network (RPN) to propose candidate regions of interest (ROI); the second uses a (convolutional) backbone to extract features which are then used to perform object classification and bounding box regression, as well as prediction of a binary segmentation mask. The former is performed via fully connected layers on the extracted features, while the latter uses further convolutional layers. In practice, learned features are shared by both stages to speed up processing.

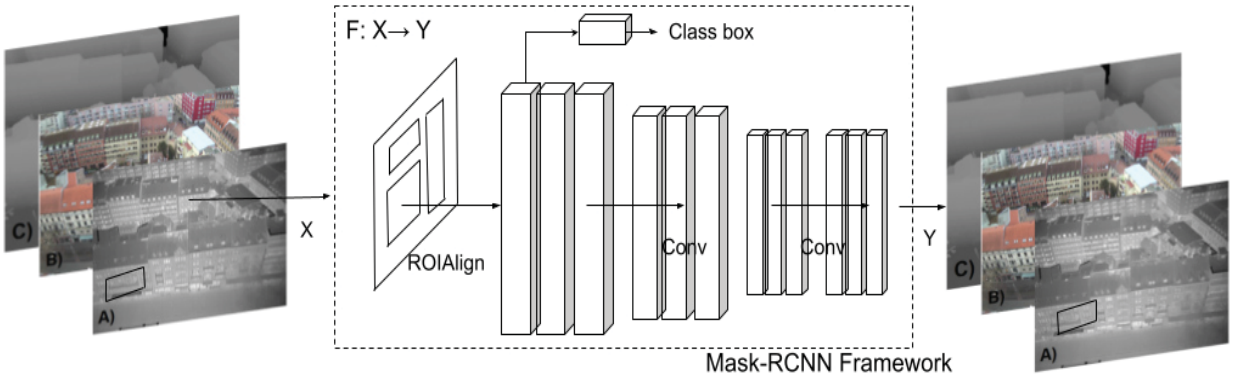

Figure 3: The Mask R-CNN framework

Mask R-CNN uses a multi-task loss on every proposed region of interest: $L = L_{cls} + L_{box} + L_{mask}$. L_{cls} is the categorical cross-entropy loss across $K + 1$ output predictions for K component classes, plus an additional catch-all class for proposed regions containing only background. L_{box} is the bounding box regression (mean squared error) over the predict box corners. L_{mask} is the average binary cross entropy across all pixels in the mask. These are described in further detail in He et al. (2017). Note that for the experiments reported in this work we use a single annotation class (i.e. K=1).

The dataset images were split into 717 training images and 200 test images corresponding to five and one of the city blocks described in the section above, respectively. Training was performed for 30,000 iterations at a batch size of eight, with random weight initialisation (i.e. no pre-training). The remaining hyper-parameter configurations were set to the Detectron2 defaults for the "mask_rcnn_R_50_FPN_3x_gn" model from the Detectron2 model zoo templates, with only changes the number of ResNet layers (18) and the pixel value means (130, 135, 135, 118, 118) and standard deviations (44, 40, 40, 30, 21) for (B, G, R, thermal, height) used by Detectron2 to normalise the inputs. These values were calculated from the full set of training images.

6. Results

To evaluate the performance of our training, we use the Average Recall (AR) metric, defined as:

$$AR = \frac{TP}{TP+FN} \tag{7}$$

where TP and FN refer to the number of true positive and false negative object predictions, respectively. The AR measures the probability of objects in an image being detected. Since not every thermal bridge in the dataset is annotated, we do not report any metrics that work with false positives (such as Average Precision). These metrics are guaranteed to underperform as even correctly predicted thermal bridges will be reported as false positives if the corresponding annotation does not exist.

To determine which predicted bounding boxes correspond to correct predictions, the Intersection-over-Union (IoU) is measured between the predicted and ground truth boxes as:

$$IoU = \frac{area(predicted \cap true)}{area(predicted \cup true)} \tag{8}$$

For a given IoU threshold, predicted bounding boxes that have an IoU with an annotated thermal bridge's bounding box above the threshold are considered true positives. Any annotated thermal bridges without a prediction satisfying this are considered false negatives. Table 1 shows the metric scores for various common variants of the AR metric. An IoU range (i.e. IoU=0.5:0.95) indicates the AR is averaged over the given interval. An area of medium or large corresponds to objects of area between 32^2 and 96^2, and greater than 96^2 pixels, respectively. Max. detections indicates the score given the N highest confidence predictions[4].

We note immediately the comparatively low scores, which we attribute to the low number of annotated examples relative to the large image sizes and sparsity/small size of thermal bridges. Notably, the network performs better at larger scales, which is likely due to larger

[4]Although often reported in object detection tasks, we do not report small (less than 32^2 pixels) thermal bridges as the smallest present in our dataset is 55^2 pixels.

thermal bridges being less ambiguous with regards to non-thermal bridge heat spots in an image.

An interesting result, however, is the location of predicted thermal bridges, regardless of their accuracy. All predictions are on or overlapping with rooftops, indicating the network has an awareness of sensible locations for thermal bridges. We find that this result is consistent across all test images. We posit that this is due to the inclusion of the height map as a signal to the neural network of where to look for thermal bridges. We plan to perform further ablation studies to confirm this.

Given the dataset was produced by a single fly over of six city blocks, some portions of the test dataset images are also present in the training images from different angles. In these instances we note that the neural network has overfitted those thermal bridges and predicts them with at or near 100% confidence. Nonetheless, the network is able to identify thermal bridges unique to the test dataset, albeit with lower confidence and IoU. We expect this to improve with the training techniques discussed in the next section.

Table 1: Bounding box regression metrics on the test images dataset

Metric	Area	Max. detections	Score
AR @ IoU=0.50:0.95	All	1	0.052
AR @ IoU=0.50:0.95	All	10	0.142
AR @ IoU=0.50:0.95	All	100	0.142
AR @ IoU=0.50:0.95	Medium	100	0.114
AR @ IoU=0.50:0.95	Large	100	0.196

7. Discussion

The Average Recall achieved is not currently suitable for thermal bridge detection; however it does provide a baseline score for prediction with a modern computer vision approach directly on the TBBR dataset. This represents a departure from previous approaches which relied on complex multi-stage solutions (as in Rakha et al. (2018)) or fine-tuning of clustering and feature extraction preprocessing steps (as in Kim et al. (2021)).

A key limitation in this work is the comparatively small number of images available for training. This is due to the time required to manually annotate each image. While we used a total of 917 images, common benchmarks often contain hundreds of thousands (e.g. COCO) or even tens of millions (e.g. Imagenet) of images.

We therefore plan to implement a self-supervised pretext task to maximise the use of collected images. Specifically, we intend to utilise the work from Hou et al. (2021 - b) to first train a neural network to predict thermal images from RGB and use these predicted images, along with the real thermal and the height information, as input to the Mask R-CNN network. This approach is similar to that of the Split-Brain Autoencoder described by Zhang et al. (2017). We hypothesise that the predicted thermal images will be nearly identical to the real thermal images, with only the thermal bridges missing[5], thus simplifying the network's task significantly to learn to locate the appropriate differences between the two. If successful, this

[5] The assumption here is that thermal bridges are only visible from the thermal image, which is of course the original motivation for including thermal images in this project in the first place.

would allow full use of all (non-blurry) drone images captured, not only those on which the laborious task of annotation has been performed.

In order to increase the size of the dataset, it is also possible to use panorama images collected from other sources. Since our approach is based on qualitative thermography, the weather conditions and temperatures when recording new images do not have to be identical to the existing dataset (Volland et al., 2016). However, the temperature contrast of new annotated thermal bridges should be high enough to detect, which is the case when there is a difference of more than 10°C between indoor and outdoor temperatures. The distances of the drone to the buildings can also vary, however thermal images with more than 20m distance to the measurement object should be checked in all individual cases for appropriate quality (Fouad and Richter, 2012).

8. Conclusion

We have reported an overall average recall of 14.2% at IoU:0.5-0.95, and 19.6% at IoU:0.5-0.95 for large thermal bridges. We demonstrated the ability of the neural network to propose predictions in reasonable locations (i.e. rooftops only) which we posited is due to the addition of height information to the input images. While this work has shown a promising first result in identifying individual thermal bridges from drone images, we believe there is still significant potential for improvement to be made using a self-supervised pretext task to maximise the information obtain from the entire set of collected images.

This work focuses on a cost-effective and scalable approach to assess thermal bridges using thermographic images from drones. In future, we intend to use financial and environmental criteria to estimate which buildings in a district the retrofit of thermal bridges is recommended and when buildings should be retrofitted more extensively.

Acknowledgements

This project was performed during a PhD project that is financed with a scholarship according to Landesgraduiertenförderungsgesetz (LGFG), the State Graduate Promotion Act, of the Karlsruhe Institute of Technology (KIT). This work is supported by the Helmholtz Association Initiative and Networking Fund, the Helmholtz AI platform grant, and the HAICORE@KIT partition. Furthermore, we thank Marinus Vogl and the Air Bavarian GmbH for their support with equipment and service for the recording of images and Tobias Beiersdörfer who supported us with the development of the TBBR dataset.

References

Begleitforschung Energetische Stadtsanierung (BES) (2020): 3. Fachkonferenz der Begleitforschung zum KfW-Förderprogramm Energetische Stadtsanierung Energiewende im Quartier (English: 3rd specialist conference of the accompanying research to the KfW funding program ‘Energy transition in districts‘). Berlin.

Bello, I. et al. (2021). Revisiting resnets: Improved training and scaling strategies. arXiv preprint arXiv:2103.07579.

Garrido et al. (2018). Thermal-based analysis for the automatic detection and characterization of thermal bridges in buildings. Energy and Buildings, 158, 1358–1367. Doi: https://doi.org/10.1016/j.enbuild.2017.11.031

Global Alliance for Buildings and Construction (GlobalABC) (2018). 2018 Global Status Report Towards a zero-emission, efficient and resilient buildings and construction sector. ISBN No: 978-92-807-3729-5.

He, K. et al. (2017). Mask r-cnn. In Proceedings of the IEEE international conference on computer vision (pp.2961–2969).

He, K. et al. (2016). Deep residual learning for image recognition. In Proceedings of the IEEE conference on computer vision and pattern recognition (pp.770–778).

Hou, Y. et al. (2021 - a). Automation in Construction Fusing tie points - RGB and thermal information for mapping large areas based on aerial images: A study of fusion performance under different flight configurations and experimental conditions', Automation in Construction. Elsevier B.V., 124. Doi: 10.1016/j.autcon.2021.103554.

Hou, Y. et al. (2021 - b). A Novel Building Temperature Simulation Approach Driven by Expanding Semantic Segmentation Training Datasets with Synthetic Aerial Thermal Images. Energies, 14(2). Doi: https://doi.org/10.3390/en14020353

International Energy Agency (IEA) (2014). Energy technology perspectives 2014: Harnessing electricity's potential. OECD/IEA.

Kim, C. et al. (2021). Automatic Detection of Linear Thermal Bridges from Infrared Thermal Images Using Neural Network. Applied Sciences, 11(3), 931. Doi: https://doi.org/10.3390/app11030931

Macher, H. et al. (2020). Automation of Thermal Point Clouds Analysis for the Extraction of Windows and Thermal Bridges of Building Facades. The International Archives of Photogrammetry, Remote Sensing and Spatial Information Sciences, 43, 287–292. Doi: https://doi.org/10.5194/isprs-archives-XLIII-B2-2020-287-2020

Martinez-De Dios, J. R., and Ollero, A. (2006, July). Automatic detection of windows thermal heat losses in buildings using UAVs. In 2006 world automation congress (pp.1–6). IEEE. Doi: 10.1109/WAC.2006.375998

Mayer, Zoe, Hou, Yu, Kahn, James, Beiersdörfer, Tobias, & Volk, Rebekka. (2021). Thermal Bridges on Building Rooftops - Hyperspectral (RGB + Thermal + Height) drone images of Karlsruhe, Germany, with thermal bridge annotations (Version 0.1.0) [Dataset]. Zenodo. http://doi.org/10.5281/zenodo.4767772

Neußer, W. (2017). Energetische Quartierssanierung - Ausblick und externe Rahmenbedingungen. (English: District energy improvement - outlook and external conditions.) Information zur Raumentwicklung, 4/2017. BBSR.

Power, A. (2008). Does demolition or refurbishment of old and inefficient homes help to increase our environmental, social and economic viability. Energy Policy 2008;36: 4487–4501. Doi: https://doi.org/10.1016/j.enpol.2008.09.022

Rakha, T. et al. (2018). Heat mapping drones: an autonomous computer-vision-based procedure for building envelope inspection using unmanned aerial systems (UAS). Technology| Architecture+ Design, 2(1), 30–44. Doi: https://doi.org/10.1080/24751448.2018.1420963

Ren, S. et al. (2016). Faster R-CNN: towards real-time object detection with region proposal networks. IEEE transactions on pattern analysis and machine intelligence, 39(6), 1137–1149. arXiv:1506.01497

Riechel, R. (2016). Zwischen Gebäude und Gesamtstadt: das Quartier als Handlungsraum in der lokalen Wärmewende. (English: Between the building and the city as a whole: the district as field for action in the local heat transition.) Vierteljahrshefte zur Wirtschaftsforschung, 85(4), 89–101.

Schild, K. (2018). Wärmebrücken: Berechnung und Mindestwärmeschutz. (English: Thermal bridges: Calculations and minimum requirements) Springer-Verlag. Doi: 10.1007/978-3-658-20709-0

Schmidt P. and Windhausen S. (2018) Bauphysik-Lehrbuch. (English: Building physics) Bundesanzeiger Verlag, Köln. Doi: https://doi.org/10.1007/978-3-658-21749-5_3-1

Volland J. et al. (2016). Wärmebrücken: erkennen-optimieren-berechnen-vermeiden. (English: Thermal bridges: recognize-optimize-calculate-avoid) 1. Auflage 420 Seiten Verlagsgesellschaft Rudolf Müller GmbH & Co. KG, 978-3-481-03365-1 (ISBN).

Wu Y. et al. (2019). Detectron2.

Zhang, R., Isola, P., & Efros, A. A. (2017). Split-brain autoencoders: Unsupervised learning by cross-channel prediction. In Proceedings of the IEEE Conference on Computer Vision and Pattern Recognition (pp.1058–1067).